INFLUENCE OF BETA-TO-ALPHA QUARTZ TRANSITION ON RESIDUAL STRESSES OF A FELDSPAR GLASS MATRIX COMPOSITE: A RELATIONSHIP WITH CATASTROPHIC FRACTURE DUE TO THERMAL SHOCK

Article reference	JECS15585
Journal	Journal of the European Ceramic Society
Corresponding author	Marcelo Dal Bo
First author	Marcelo Dal Bo
Received at Editorial Office	20 Dec 2022
Article revised	22 Mar 2023
Article accepted for publication	26 Mar 2023

ISSN 0955-2219

Last update: 26 Mar 2023

Share via email

Status comment

- Your article has been received for production.

Production events

26 Mar 2023 Received for production

Complimentary items

- You are entitled to a Share Link for your article free of charge. The Share Link will be sent you as soon as the final article is published in an issue.

Track another article >

Bibliographic information

Volume/Issue
Will appear soon

Full bibliographic details
Will appear soon

Article available online
Will appear soon

Track another article

INFLUENCE OF BETA-TO-ALPHA QUARTZ TRANSITION ON RESIDUAL STRESSES OF A FELDSPAR GLASS MATRIX COMPOSITE: A RELATIONSHIP WITH CATASTROPHIC FRACTURE DUE TO THERMAL SHOCK

Marcelo Dal Bó [a*], Francisco A. Gilabert [b], Anselmo Ortega Boschi [c], Enrique Sánchez [d], Vicent Cantavella [d], Dachamir Hotza [e]

[a] *Federal Institute of Santa Catarina (IFSC), Campus Criciúma, SC, Brazil*
[b] *Department of Materials, Textiles and Chemical Engineering, Ghent University, Ghent, Belgium*
[c] *Department of Materials Engineering (DEMa), Federal University of São Carlos (UFSCar), SP, Brazil*
[d] *Institute of Ceramic Technology (ITC), Universidad Jaume I (UJI), Campus Riu Sec, Castellón, Spain*
[e] *Department of Chemical Engineering (EQA), Graduate Program in Materials Science and Engineering (PGMAT), Federal University of Santa Catarina (UFSC), SC, Brazil*

* Corresponding author: Phone/Fax: +55 48 3462-5019
E-mail address: marcelodalbo@hotmail.com (Dal Bó, M.)

Abstract

A wide range of porcelain-based materials is composed of quartz crystalline particles dispersed in a homogeneous glassy phase. During the cooling stage these composites are subjected to stresses related to the transition from β to α quartz at 573 °C. This work studies, numerically and experimentally, the influence of the cooling rate, the quantity, and the size of the quartz crystalline particles on the stresses suffered by the material throughout the cooling process. This procedure allows calculating the instantaneous profile of stresses through the cross-section specimen during the whole cooling stage. For this, a dense glass matrix from sodium feldspar was prepared. The results reveal that the evolution of the stress profile is strongly affected by the cooling rate. The evolution of the tension state in the sample during the cooling can help to understand the catastrophic fracture suffered during the β to α quartz transition related to thermal shock.

Keywords

Residual stresses, thermal tempering, constitutive modeling, quartz, ceramic composites.

Contents

Abstract 1
Keywords 1
1. INTRODUCTION 3
2. THEORETICAL BACKGROUND 4
2.1. Experimental theory 4
2.2. Simulation theory 5
3. MATERIALS AND METHODS 6
3.1. Specimen preparation 6
3.2. Thermomechanical properties of the composite materials 9
3.2.1. Effective thermal diffusivity evaluation 10
3.2.2. Viscosity measurements 11
3.2.3. Thermal expansion measurements 12
3.2.4. Young's modulus measurements 13
3.3. Microstructural characterization 14
4. RESULTS AND DISCUSSION 15
4.1. Characterization of pure feldspar glass and the composites 15
4.2. Results of thermal calculations 16
4.3. Surface residual stresses at room temperature 17
4.4. Evolution of surface stress during cooling 19
4.5. Processing-microstructure-properties correlation 24
5. CONCLUSIONS 26
Acknowledgments 27
References 27

1. INTRODUCTION

The sintering process of ceramic materials is a thermal treatment consisting of an initial heating, a hold at maximum temperature for a certain time, and a final cooling stage, whose rate can be varied [1]. According to the cooling rate, macroscopic stresses can be generated in the material that can either lead to catastrophic fracture of the material, due to the so-called thermal shock [2], or increase the mechanical strength of the material, in a process known as thermal tempering [3,4]. Therefore, controlling the cooling rate and the material properties that influence this process are essential to promote residual compressive stresses at the surface of the material, without causing a catastrophic fracture.

The advantages of thermal tempering are twofold: (*i*) the production process is accelerated significantly, and (*ii*) the material's mechanical performance can be improved thanks to the presence of compressive residual stresses on the surfaces of the specimen [5-7].

Porcelain tiles sintered under fast cooling rates have presented an increase in the macroscopic compressive residual stresses at the surface [7-10]. This feature was evidenced through a remarkable increase of the breakage strength and is the same as that generally found in most glasses when they are subjected to a tempering process [3,4]. The generation of macroscopic residual stresses has been also found in other materials, such as dental porcelain [11,12], ceramic laminate composites [13,14], thermoplastics [15,16], and metals [17,18].

The aim of this work consists of the development and validation of a numerical method capable to predict complete information concerning the stresses generated within the material during the cooling stage. To carry out these computations, the model needs as input data the whole set of thermomechanical properties of each composition constituent. The mathematical formulation of this model is based on two steps: (*i*) initially the thermomechanical properties of the material are studied, providing the calculation of the temperature profile of the material throughout the cooling process, and (*ii*) the second step uses a viscoelastic model of ceramic materials to calculate the deformation of the material, relating with the stresses during the cooling. The respective theoretical fundamentals can be found in [19-21]. For the validation of the numerical part of the work, the residual stresses profile in the cross section of the ceramic material was measured using the Strain Relaxation Slotting Method (SRSM) [22]. Those theoretical aspects are better explained in the following section.

2. THEORETICAL BACKGROUND

2.1. Experimental theory

The relaxation methodology by incremental cut was used to obtain the experimental macroscopic residual stresses in a cross section of the ceramic materials. This approach consists of the adhesion of an extensometer to a specimen with subsequent incremental cuts with a known size (a_i) (Figure 1), measuring the extensometer deformation (ε_{gi}) [22-24]. The free extensometer deformation (ε_f) can be decomposed by a linear combination of Legendre Polynomials (P_k), shown in Equation 1:

$$\varepsilon_f = \sum_{k=0}^{n_p-1} \lambda_k P_k(\zeta) \tag{1}$$

where: n_p is the number of Legendre polynomials; ζ is the coordinate at thickness direction (ζ = -1 for below surface and ζ = 1 for top surface); and λ_k are the Legendre polynomial coefficients (unknown).

Values of λ_k can be found from a_i and ε_{gi} with the application of a "calibration function" previously determined by finite element calculations [22]. This variable is dependent on the specimen geometry and the relative cut or extensometer position. Since λ_k can be calculated, the macroscopic residual stresses profile around a cross section of specimen σ_r (z) can be established from a simple relationship between the deformation and the elastic modulus (E) of the material. Furthermore, in ceramic materials, the residual stresses can be usually described using only the term of the second degree, as presented in Equation 2.

$$\sigma_r = -E\sum_{k=2}^{\infty} \lambda_k P_k(\zeta) \cong -E\lambda_2 P_2(\zeta) = \sigma_{sfc} P_2(\zeta) = \sigma_{sfc} \frac{3\zeta^2 - 1}{2} \tag{2}$$

The residual stresses at the surface are $\sigma_{sfc} = -E\lambda_2$. Therefore, the full profile of residual stresses can be described only as a function of the surface stress.

Figure 1 and Figure 2 show the incremental cut and the specimen deformation according to the stress relaxation, respectively.

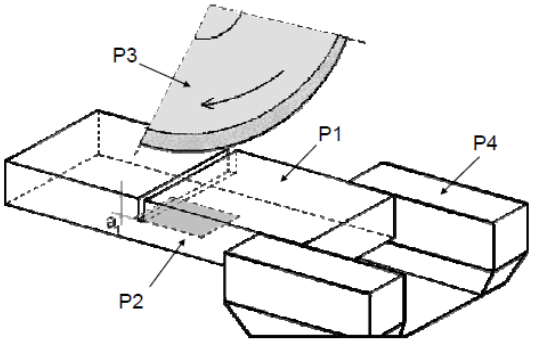

Figure 1. Experimental illustration of a strain relaxation slotting method: Specimen (P1); Gauge (P2); Cut disc (P3) and Clamp (P4) [25].

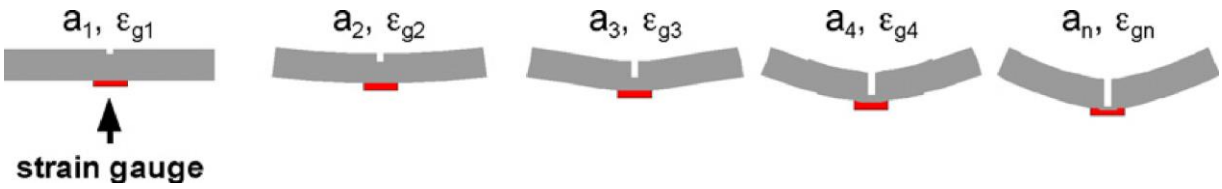

Figure 2. Foundations of the strain relaxation slotting method [7].

2.2. Simulation theory

The theoretical model [19] is developed in two steps, as illustrated in Figure 3. The first step is related to the solution of the thermal problem so that the temperature profile in the specimen is calculated. Therefore, it is necessary to know the specimen geometry, the respective thermal properties (thermal conductivity and specific heat), the bulk density, and the surface temperature during cooling.

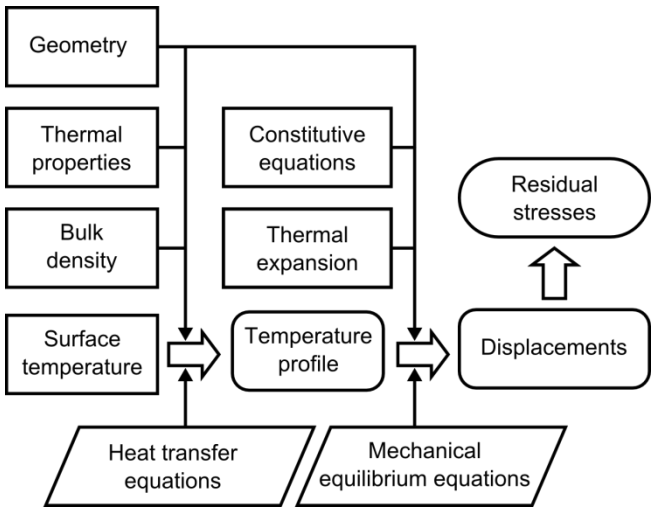

Figure 3. Steps of the theoretical model.

The equation of heat transfer in unsteady state takes the form [20]:

$$\frac{\partial T}{\partial t} = \alpha \nabla^2 T \quad (3)$$

where T is the temperature (K) in a point of the specimen at a determinate time; t is the time (s); and α is the thermal diffusivity (m^2/s). The latest property is the relationship between the thermal conductivity (k), bulk density (ρ), and the heat specific (C_p), given as $\alpha = k/(\rho C_p)$.

The second step is related to solving the mechanical problem, determining the displacement of each specimen point including mechanical properties, dilatometric curve, equilibrium equation, and the thermal profile.

The mechanical equilibrium equations come from the balance of forces and momenta applied to the specimen [21] and, thus, are not dependent on the material's type or properties. The behavior law establishes a relationship between the tensile and deformation of the material and the function of the kind of material. A simple law is the Hooke equation (linear elasticity); however, this law is not suitable to explain the stress generation during materials cooling. A non-elastic component is needed, for example, the linear viscoelastic, as shown in Equation 4:

$$\varepsilon_{e,x} = \frac{1}{E}\sigma_x$$
$$\frac{d\varepsilon_{v,x}}{dt} = \frac{1}{3\eta}\sigma_x \quad (4)$$

where $\varepsilon_{e,x}$ is the elastic deformation along the x axis; $\varepsilon_{v,x}$ is the viscous deformation along the x axis; σ_x is the normal tensile on a perpendicular plane at the x axis (Pa); E is the elastic modulus (Pa); and η is the viscosity (Pa·s).

There are many relationships of a glass viscosity (η) as a function of the temperature (T), such as the Arrhenius equation [26]:

$$\eta = \eta_0 e^{\Theta/T} \quad (5)$$

where η_0 is the pre-exponential factor (Pa·s); and Θ a constant (K).

To solve the thermal and mechanical problems, numerical methods are usually applied: finite differences and finite element methods were used for thermal and mechanical calculations, respectively.

3. MATERIALS AND METHODS

3.1. Specimen preparation

A dense glass matrix composed mainly of sodium feldspar (albite, Mario Pilato, Spain) was developed to study the residual stresses. The initial size of feldspar powder particles was reduced by wet milling in a planetary mill with alumina balls for 30 min,

resulting in a D_{50} around 6 μm. Once the feldspar powder was dried, it was granulated using an 8 wt.% aqueous solution with 5 wt.% PVA (polyvinyl alcohol). The resultant material was pressed using a pressure of 35 MPa.

Additionally, two quartz types were used: SE-100 and SE-8 (both from Sibelco, Belgium). From the combination of feldspar and quartz, 5 compositions were formulated (Table 1): (A) composed solely by sodium feldspar; (B) sodium feldspar with 18.5 vol.% quartz SE-100; (C) sodium feldspar with 18.5 vol.% quartz SE-8; (D) sodium feldspar with 37.6 vol.% quartz SE-100; (E) sodium feldspar with 37.6 vol.% quartz SE-8.

Table 1. Materials developed in this work.

Material	**Sodium feldspar**	**Quartz**		
	(vol.%)	**(vol.%)**	**Type**	**Particle size (D_{50}, μm)**
A	100	---		---
B	81.5	18.5	SE-100	13.4 ± 0.6
C	81.5	18.5	SE-8	31 ± 4
D	62.4	37.6	SE-100	13.4 ± 0.6
E	62.4	37.6	SE-8	31 ± 4

The different compositions were developed to alter the size and quantity of crystalline quartz particles dispersed in the albite glass phase. The quartz particles were mixed by wet milling with alumina balls for 10 min into the previously ground feldspar. After homogenization, the material was dried, granulated, and pressed in the same way as mentioned before.

An X-ray diffractometer (XRD, Bruker Theta-Theta, model D8 Advance) was used to determine the crystalline phases. The measurement parameters were varied depending on each sample: voltage (30 to 40 kV), current (40 to 45 mA), time (0.5 to 1.2 s), step size (0.015 to 0.02°), and 2θ angle (5º to 90º). The crystalline phases were quantified by the Rietveld method, using fluorite as internal standard.

Sintering was carried out in an electric furnace (Pirometrol R-series), with a first heating rate of 3.5 ºC/s between 25 and 500 ºC, followed by a heating rate of 0.4 ºC/s until

reaching the maximum densification, which occurred at 1200 ºC for materials A, B and C and at 1250 ºC for materials D and E. This temperature was held for 6 min, followed by three different cooling rates:

- *Slow Cooling (SC),* which was carried out in the furnace, and corresponded to a slow rate of cooling (Figure 4, green curve);
- *Mixed Cooling (MC)* was divided into two steps; the first at a slow cooling in the furnace from maximum densification temperature up to 650 ºC; a fast cooling followed to room temperature (Figure 4, blue curve), using the equipment shown in Figure 5;
- *Fast Cooling (FC)*, which consisted of rapid extraction of the specimens from the furnace at maximum densification temperature, and subsequently forced ventilation using 1 bar of air pressure, with the equipment shown in Figure 5; this procedure resulted in a fast cooling rate (Figure 4, red curve).

The three cooling methods aimed to promote (or not) the generation of residual stresses. The surface temperature of the specimens was measured with a pyrometer (Raytek, model MI320LTS), as a boundary condition to calculate the temperature profile in the cross section of ceramic materials.

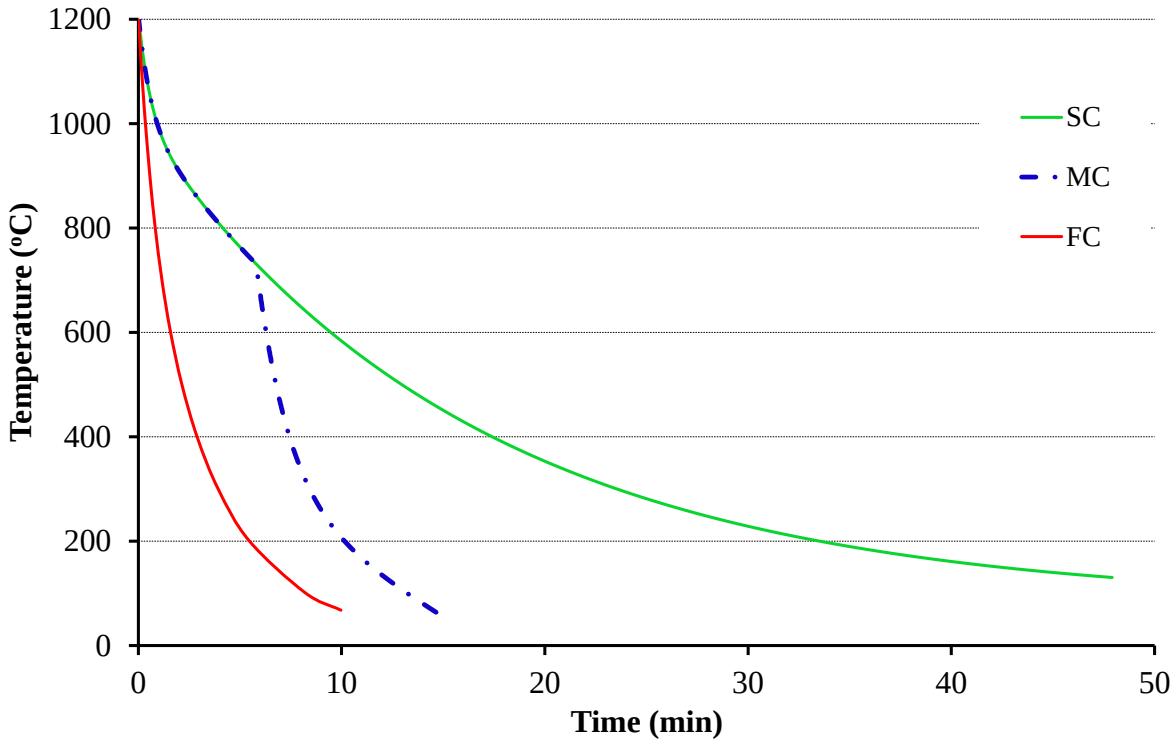

Figure 4. Cooling rates used in this work: slow cooling (SC), mixed cooling (MC), and fast cooling (FC).

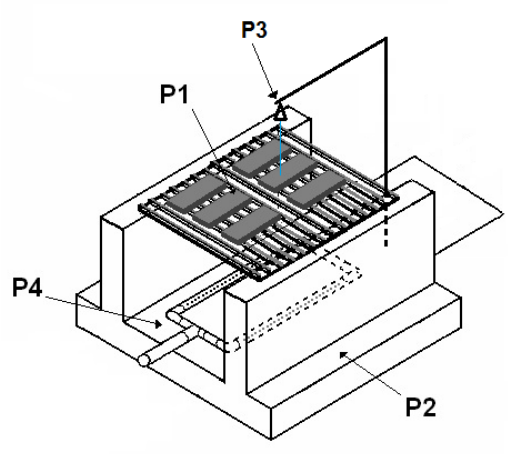

Figure 5. Equipment developed to perform the quenching of ceramic samples, composed of a refractory plate (P1), refractory support (P2), pyrometer (P3), and forced ventilation (P4) [7].

3.2. Thermomechanical properties of the composite materials

For the numerical determination of the stress profile in ceramic materials, it is necessary to know their related thermomechanical properties [27]:

- Thermal effective diffusivity (D_{eff}) of the ceramic composite (glass matrix and crystalline particles) with the temperature variation;
- The viscosity (η) of the heterogeneous ceramic materials in molten state with the temperature variation;
- Coefficient of thermal expansion (α), from room temperature to the maximum sintering temperature;
- Elastic modulus (E) according to the temperature variation.

The thermal expansion was measured using a contact dilatometer (Adamel-Lhomargy, model DI-24), which was calibrated with a sapphire standard. Previous works [26-35] allowed the determination of the thermal effective diffusivity of materials. The elastic modulus was determined within the temperature range 25-700 ºC with an impulse excitation technique device (Grindosonic). Above the glass transition temperature (T_g), a relationship was found to Young's modulus behavior and applied [36]. The viscosity was obtained according to previous works on sodium feldspar thermal properties [26,31]. However, solid particles (crystals) were included by using the Krieger-Dougherty relationship [37,38]. Experimental viscosity verification was performed with a noncontact dilatometer (Misura HSM, model M3M1600.80.2). The thermomechanical properties of all materials were evaluated according to their composition after sintering, since the behavior of residual stresses studied in the work is generated during the cooling step. The evaluation of each thermophysical property is discussed below.

3.2.1. Effective thermal diffusivity evaluation

Ceramic materials can present a microstructure composed of a glassy matrix and randomly scattered crystals. Thus, the consideration of thermal diffusivity of a homogeneous and uniform component becomes erroneous. In this case, the Effective Medium Theory Model (EMT) method [28-30,39] was used to determine the thermal diffusivity of a composite material composed of a glass matrix with crystalline particles and porosity. This method assumes a random distribution of components and it can be expressed as follows.

$$\sum_j v_j \frac{k_j - k_{eff}}{k_j + 2k_{eff}} = 0 \quad (6)$$

where v_j is the volume fraction of component j; K_j is the thermal conductivity of component j; and K_{eff} is the effective thermal conductivity.

The thermal conductivity and thermal diffusivity data of albite glass [31], albite crystals [31], quartz crystals [32], and air (porosity) [33] were used to calculate the effective thermal diffusivity of the studied compositions. The EMT model correlates the thermal conductivity of each component with its respective effective thermal conductivity. According to Gibert and Mainprice, the thermal diffusivity can be calculated by Equation 7 [32]. In this case, the density of each component (albite glass, albite crystals, and quartz crystals) was considered temperature dependent, and their data were found in the literature [31,34]. The heat capacity was also considered to be temperature-dependent [31,35]. Therefore, the effective thermal diffusivity of the materials was evaluated as follows:

$$D_{eff} = \frac{k_{eff}}{\rho C_p} \quad (7)$$

where D_{eff} is the effective thermal diffusivity; K_{eff} is the effective thermal conductivity; ρ is the bulk density; and C_p is the heat capacity.

Figure 6 shows the thermal effective diffusivity variation with the temperature. In this case, the D_{50} of the quartz particles had no influence on the D_{eff}.

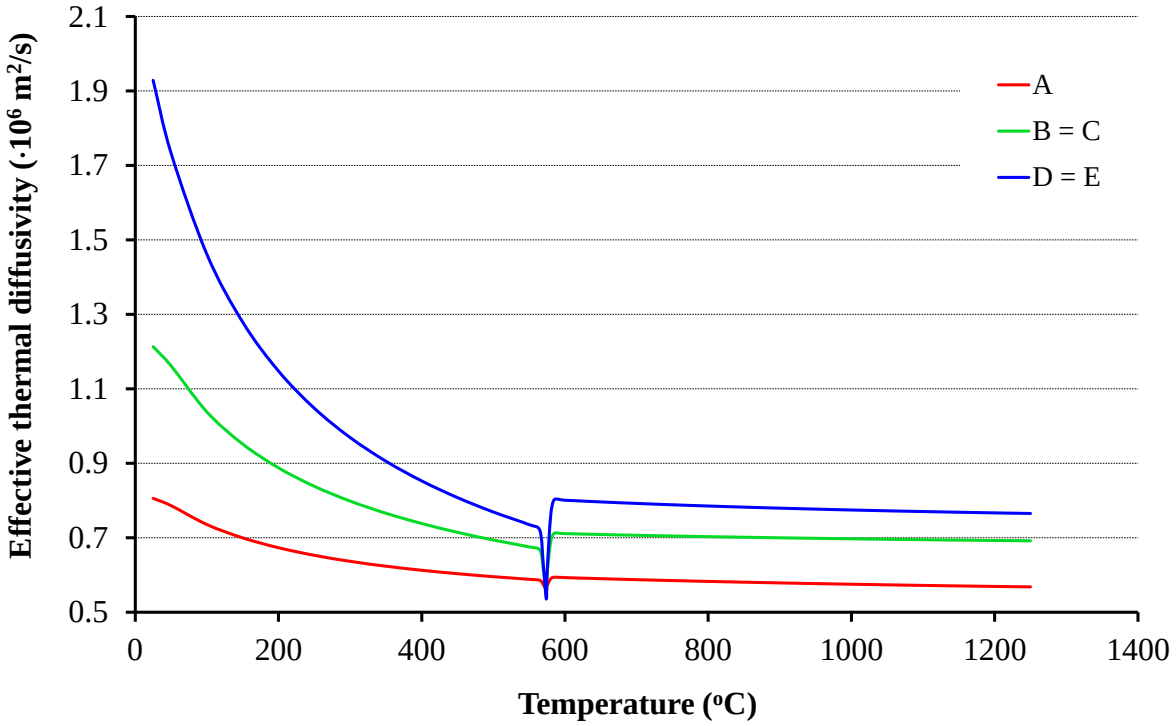

Figure 6. Effective thermal diffusivity of the composite materials.

3.2.2. Viscosity measurements

According to Scarfe and Cronin [26], the albite glass viscosity presents an Arrhenius behavior, and its activation energy is temperature-independent. Therefore, the viscosity (η) as a function of temperature (T) can be expressed by Equation 8:

$$\ln(\eta) = \ln(\eta_0) + \frac{E_a}{RT} \tag{8}$$

where η_0 is the viscosity at infinite temperature; E_a is the activation energy; and R is the universal gas constant.

Based on a Taylor viscosity model [37], Krieger and Dougherty [38] proposed a model of solid particles dispersed within a fluid. This relationship is valid for Newtonian fluids and it is represented by Equation 9:

$$\eta` = \eta\left[1 - \frac{\phi}{\phi_m}\right]^{-q\phi_m} \tag{9}$$

where η' is the viscosity within dispersed particles; q is an exponent usually equal to 2.5; φ is the particle volume fraction; and φ_m is the maximum particle value (φ_m = 0.64 in the case of a random close packing for dispersion of spherical spheres with the same diameter).

By linearizing Equation 9 and operating over Equation 8, an expression can be obtained, which correlates the viscosity with the temperature when there is a dispersed phase, namely:

$$\ln(\eta) = A` + \frac{B}{T} \tag{10}$$

where *A'* is the independent temperature term, i.e., $\ln(\eta_0) - q.\phi_m ln\left(1 - \phi/\phi_m\right)$; and *B* is the ratio between E_a and *R*.

Knowing that the albite glass presents an Arrhenius like viscosity behavior, this relationship can be described according to the literature [40,41]. Table 2 shows the results of the composite materials, where the $T_{1/2s}$ is the half sphere temperature. These results are in agreement with previous works related to albite glass viscosity [26].

Table 2. Experimental viscosity results of the composite materials .

Characteristic temperature	**Viscosity (Pa·s)**	**Material / Temperature (ºC)**				
		A	**B**	**C**	**D**	**E**
T_g	10^{12}	816	830	830	833	833
$T_{1/2s}$	$10^{3.5}$	1465	1470	1450	1540	1540

3.2.3. Thermal expansion measurements

During the initial stage of quenching, the surface cools more rapidly than the interior, and in a few seconds, the temperature difference between the surface and midplane reaches a maximum [3]. Then, the interior cools more rapidly than the surface, until isothermal conditions are established at room temperature. Therefore, the thermal shrinkage of the surface is initially greater than that of the midplane. This differential shrinkage tends to generate tensile stress at the surface and compressive stress in the midplane. The shrinkage rate is expressed by the thermal expansion coefficient of the material (α) [42].

Figure 7 shows the thermal expansion of the composite materials from room temperature to 1250 ºC. The extrapolation above T_g followed the results obtained with the optical dilatometer equipment. As can be seen, the D_{50} of quartz particles had no influence on α.

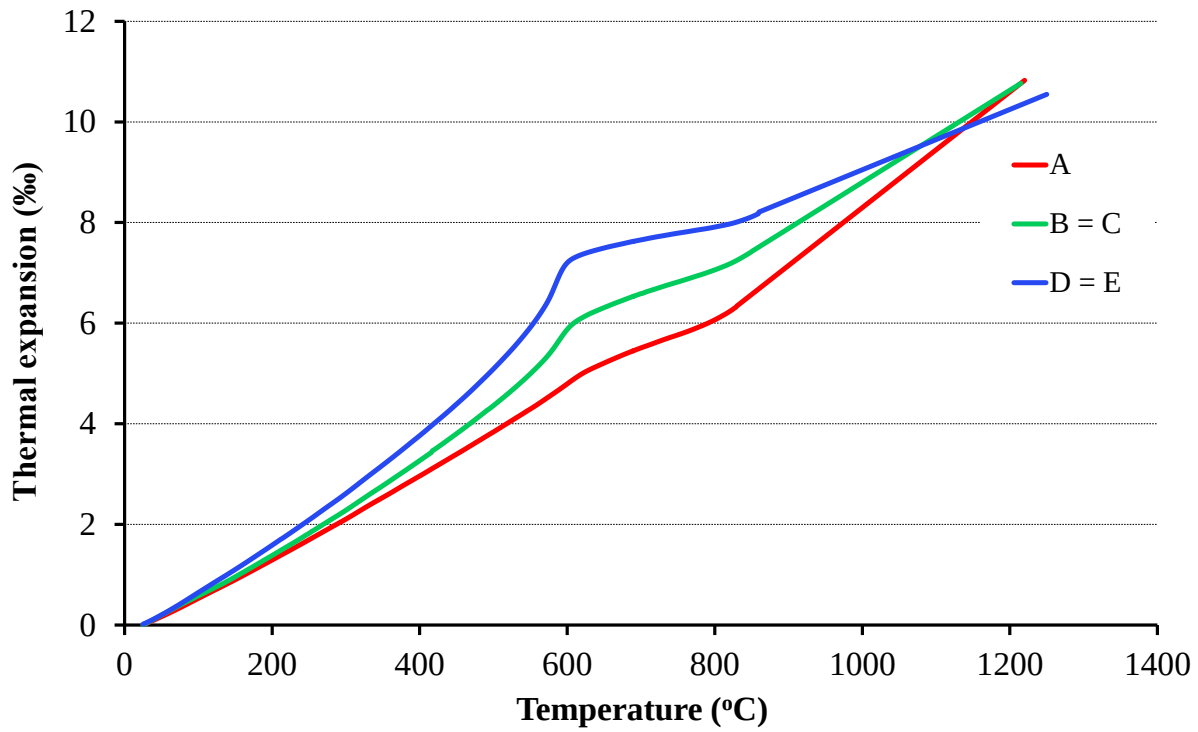

Figure 7. Thermal expansion curves of the composite materials.

3.2.4. Young's modulus measurements

The Young's modulus variation was obtained for each composite material by a nondestructive test using a device (Grindosonic) based on the impulse excitation technique [43-45]. Above T_g, the glassy behavior reported by Rouxel [36] was applied to describe Young's modulus at high temperature. Equation 11 predicts Young's modulus temperature dependence above T_g for glasses.

$$E = E_{Tg} \frac{T_g}{T} \tag{11}$$

where E is Young's modulus, E_{Tg} is Young's modulus at T_g and T is the absolute temperature (K).

The transition temperature of each material was determined by contact dilatometry. The variation of Young's modulus of quartz crystal with temperature was obtained according to Ohno *et al*. [34] and Lakshtanov *et al*. [46]. On the other hand, the data related to the albite crystal were obtained according to Ahrens *et al*. [47]. The data referring to the albite glass were obtained experimentally and published by Dal Bó *et al*. [48]. The respective Young's modulus of the tested composite materials are shown in Figure 8.

Finally, effective Young modulus (E_{eff}) following the rule of mixtures [49] for each composite, according to Equation 12:

$$E_{eff} = \sum_{j} v_j E_j \tag{12}$$

where v_j and E_j are the volumetric fraction and Young's modulus of phase j, respectively.

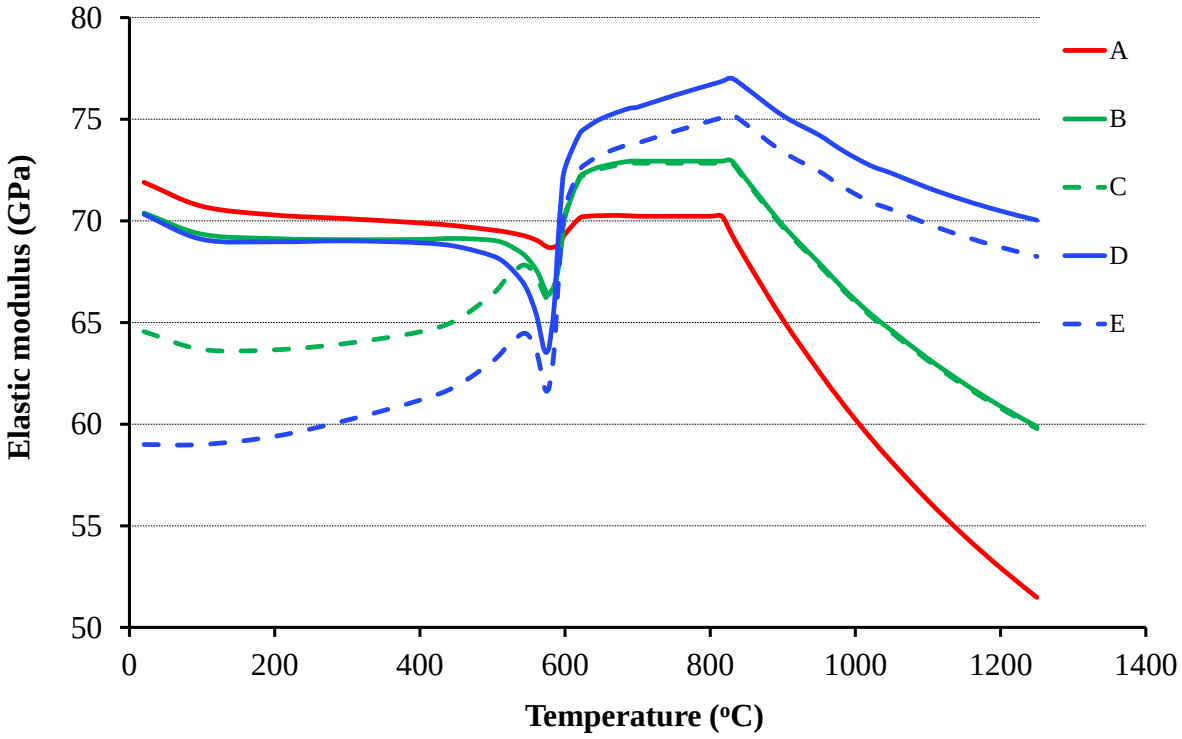

Figure 8. Young's modulus behavior of the composite materials.

3.3. Microstructural characterization

The samples were analyzed chemically, and the microstructure of the specimens was studied using a scanning electron microscope (FEI Quanta 200 ESEM FEG) coupled with a microprobe (EDAX Genesis 7000 SUTW EDX).

4. RESULTS AND DISCUSSION

4.1. Characterization of pure feldspar glass and the composites

Figure 9 and Table 3 show, respectively, the qualitative and quantitative results of crystalline and amorphous phases present in the studied materials. Material A, composed entirely of sodium feldspar, presented a high amount of albite glass. The composites B, C, D, and E showed a decrease in amorphous phase amount, which is a result of the addition of quartz crystalline particles.

As the XRD results for materials B and C were very similar, this was also reflected in the respective phase quantification by Rietveld. The same happened with materials D and E. As a result, the amount of phases present in the materials proved to have little influence from the size of the quartz used, which may be related to the short time in which the materials remained at the maximum temperature during sintering (6 min).

Table 3. Crystalline and noncrystalline phases quantification of the composite materials after sintering .

Material	**Amorphous phase**	**Crystalline phases**	
	(wt.%)	**Quartz (wt.%)**	**Albite (wt.%)**
A	78 ± 2	7 ± 1	16 ± 1
B = C	63 ± 2	28 ± 1	10 ± 1
D = E	42 ± 2	45 ± 1	12 ± 1

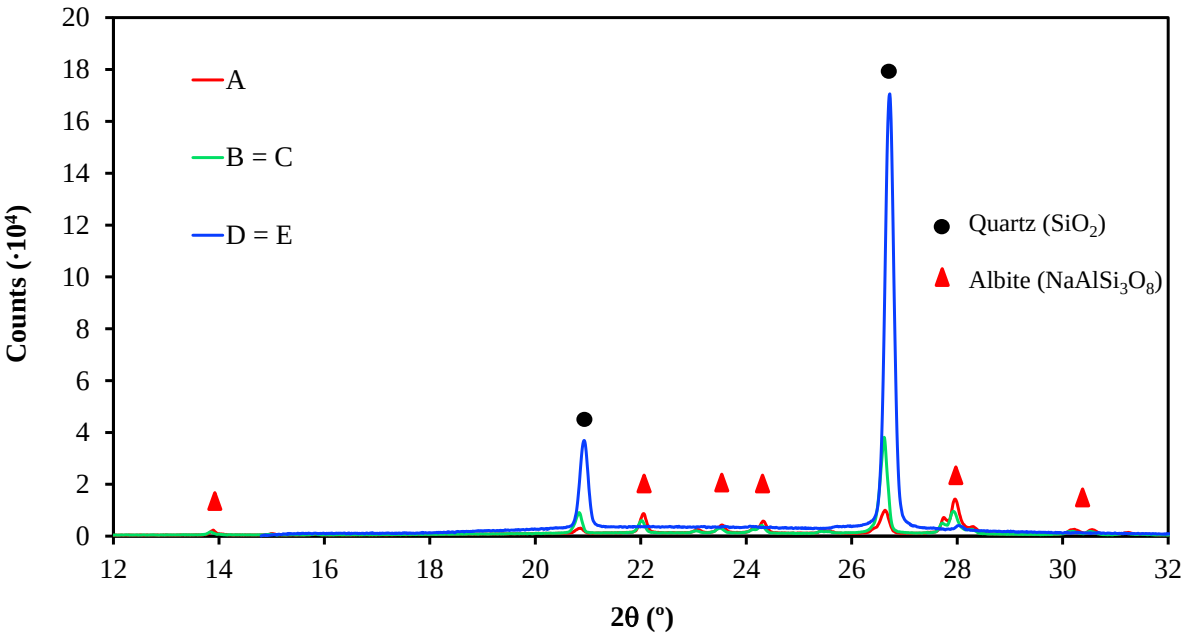

Figure 9. Diffractograms of the composite materials.

4.2. Results of thermal calculations

Figure 10 shows the results of the thermal calculations, including the temperature difference between the midplane and top surface of the specimens, according to Eq. 3 and the thermal properties of materials shown in Section 3.2. According to Narayanaswamy and Gardon [3] this temperature difference at cooling leads to a shrinkage faster at the surface than in the midplane of the sample, which is translated into permanent macroscopic residual stresses. The maximum temperature difference was obtained during an initial stage of the cooling (8 to 20 s). Material A during fast cooling (FC) presented a temperature difference of 90 ºC; while with slow cooling (SC), the maximum temperature difference was around 31 ºC. The results of thermal calculation also showed that the quartz addition decreased the temperature difference between the midplane and surface material. This result can be explained as the quartz addition increases the effective thermal diffusivity of the material (Figure 6). On the other hand, the quartz particle size did not change the effective thermal diffusivity. Thus, the temperature difference between the midplane and surface of composites B and C was the same, as well as the thermal behavior of composites D and E.

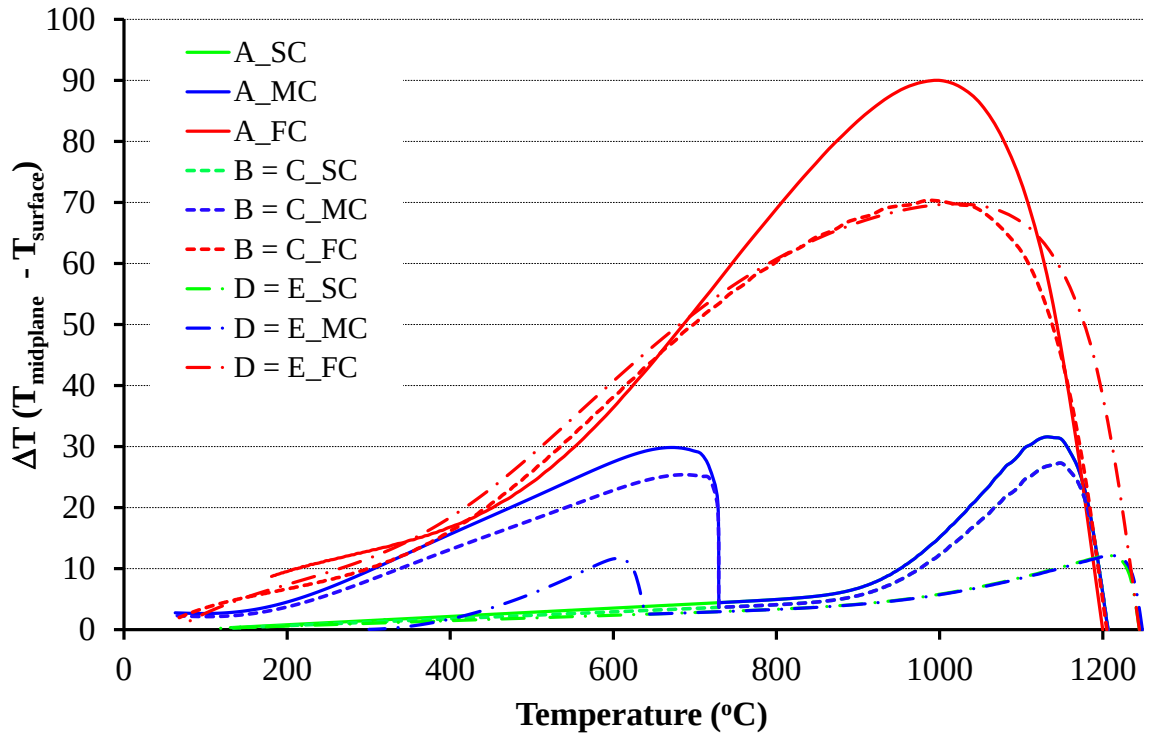

Figure 10. Temperature difference between midplane and top surface, during slow cooling (SC), fast cooling (FC) and mixed cooling (MC) of the composite materials .

4.3. Surface residual stresses at room temperature

Figure 11 compares the residual stresses results obtained experimentally and the numerical simulation results for material A, submitted to slow, mixed and fast cooling (SC, MC, and FC, respectively). The numerical simulation results were obtained from the Equations shown in Section 2.2, while the experimental results were obtained according to the procedure described in Section 2.1. The parabolic profile of the residual stresses agrees with previous works [7,11,50,51]. The residual stress profile obtained with the simulation agrees with the experimental results, for all cooling rates. When the materials were subjected to cooling that did not cause a great difference in temperature between the center and the surface, the generation of residual stresses was not observed, i.e., slow or mixed cooling (SC and MC). On the other hand, fast cooling (FC), which caused a large temperature difference between the center and the midplane of the samples, led to the generation of residual compressive stresses at the surface after the cooling was completed. Both theoretical and experimental results showed that the compression surface stress is concentrated at ~20 % of the total thickness, which is in agreement with other theoretical and experimental works [52-54]. These residual compressive stresses at the surface increase the breaking strength of the materials [7,25,55]. Therefore, material A when submitted to the fast-cooling rate presents,

theoretically, an increase of ~20 MPa when compared with the same material submitted to a slow cooling rate.

The effect of macrostresses and microstresses on the mechanical behavior of porcelain materials was investigated by Cantavella *et al.* (2008). Their work made it clear how mechanical properties, residual stresses, and cooling rate are related. Microstresses within the quartz particles were not considerably influenced by the cooling rate, while macrostress development and crack growth are significantly influenced by the cooling rate [56]. On the other hand, the findings of Dehoff *et al.* (1989), who examined the tempering stresses in feldspathic porcelain for dental applications, were comparable to those of this study, i.e., the material experienced ~20 MPa surface compression when it underwent rapid cooling [50].

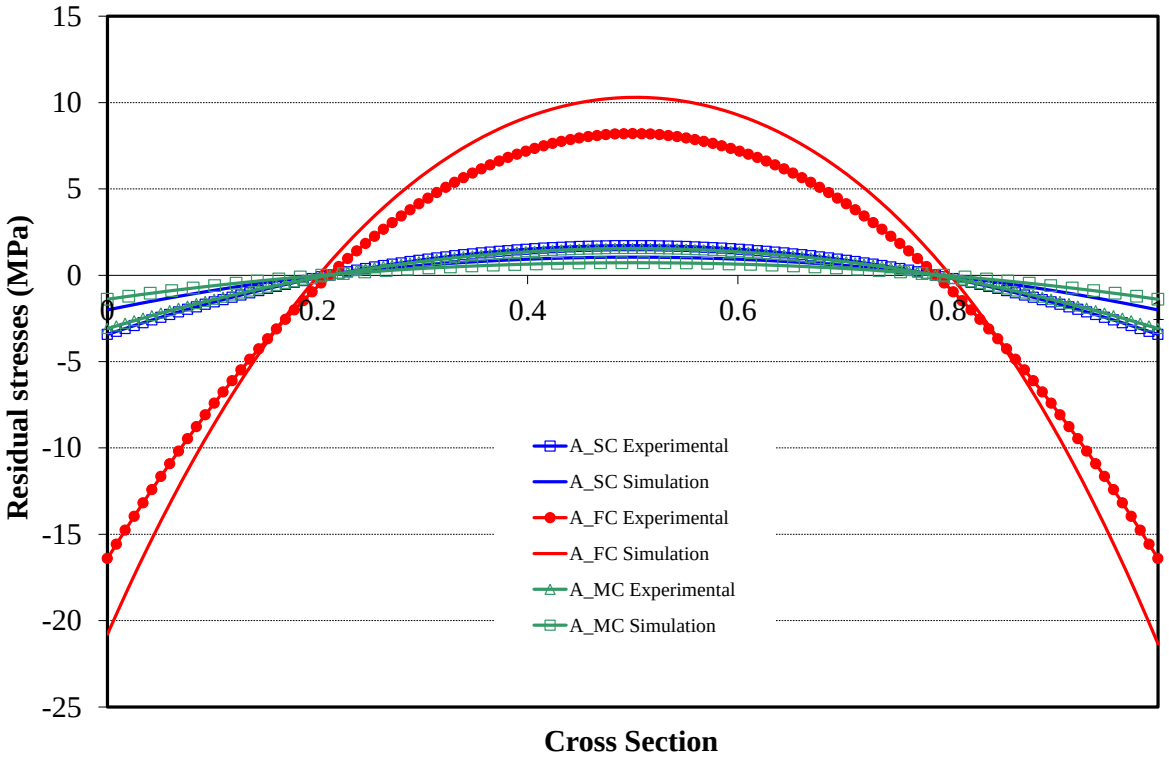

Figure 11. Comparison between the simulation and experimental results to material A , submitted to slow, fast and mixed cooling (SC, FC, and MC, respectively).

Figure 12 shows the residual stresses for each studied material. The results showed adequacy between the residual stresses experimentally measured by the SENB method and those theoretically calculated by the proposed mathematical model. Generally, the results indicate that the quartz addition decreases the macroscopic residual stresses at the material surface. This behavior can be explained by the changes in the thermomechanical properties of the ceramic materials. Furthermore, it can be observed that the variation of the crystalline quartz particle size did not change the residual stresses at room temperature. This is due to

this variation that does not strongly affect the thermomechanical properties, as seen before in item 3.2 of this work.

To all materials submitted to mixed cooling (MC), the theoretical and experimental results show that there was no generation of high residual stresses, confirming that the residual stresses are generated at high temperatures, i.e., above the glass transition temperature of each material. Similar results were also found in a previous work [25], in which the residual stress generation occurred between 1200 and 650 ºC.

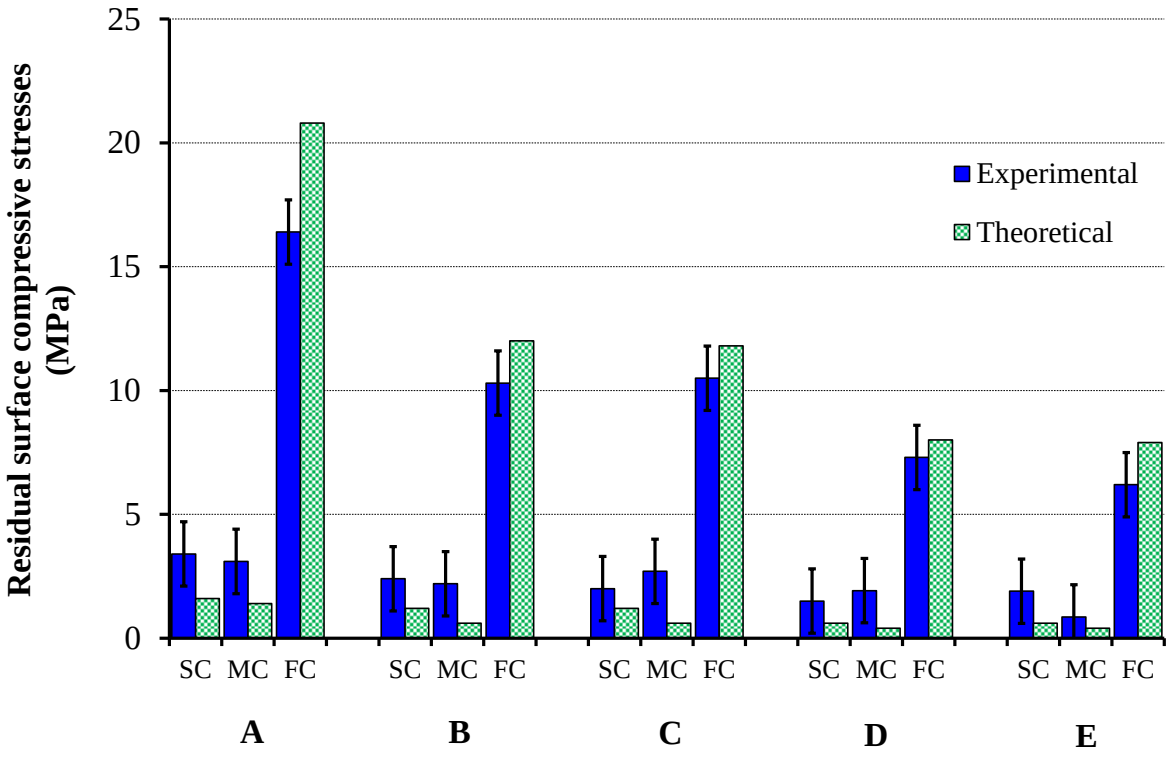

Figure 12. Results of the residual surface stresses related to slow, mixed and fast cooling rates (SC, MC, and FC, respectively) studied for composite materials .

4. 4. Evolution of surface stress during cooling

After the mathematical model has been validated with the aid of the experimental measurement of residual stresses, the mathematical tool developed can then be used to study the behavior of the stresses undergone by the material throughout the entire cooling process of the ceramic material. In this sense, Figure 13 shows the stress evolution during the SC, MC, and FC for each material. According to the numerical simulation, the material surface is not subjected to stress at temperatures between 1200 and 862 ºC, due to the viscoelastic behavior of the glassy phase. Therefore, all thermal and viscoelastic stresses generated in

this temperature range are relaxed during a time less than 1 s, which was the condition used for the numerical simulation.

Also, according to Figure 13, the residual stresses increase at a temperature very near the T_g of the glassy phase (albite glass, in this case), i.e., around 816 ºC, as Table 2 and Figure 7 show. The quartz β to α transition (573 ºC) affected the stress during cooling, showing that changes in thermomechanical properties of material during the quartz transition affect the stress magnitude at the surface of the materials. For material A, this behavior can be seen even with a low quartz amount (6.8 wt.% as indicated in Table 3). The influence of the β to α quartz transition is more pronounced when a higher cooling rate is used, i.e., FC and MC.

The quartz transition influences the stress because, during cooling, there is a high temperature difference between the midplane and surface of the composite material. In this case, the quartz crystalline particles close to the surface present the β to α quartz transition earlier than the particles near the midplane. During SC, the quartz transition had little effect on the stresses, due to the greater homogeneity of temperatures between the center and the interior of the material. Another important fact to be highlighted is that, during the quartz transition, the surface of ceramic materials was subjected to a state of traction. Exceptions were found only for material A when submitted to SC and FC.

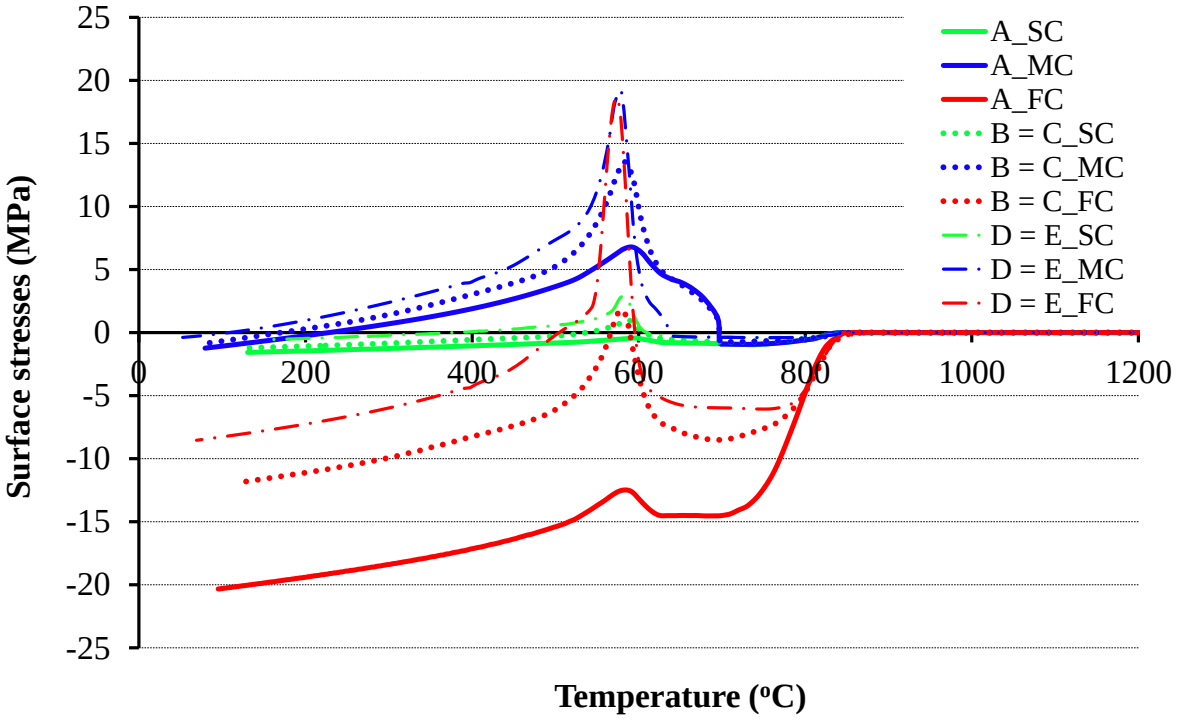

Figure 13. Surface stress evolution during slow, mixed and fast cooling rates (SC, MC, and FC, respectively) for composite materials .

The normalized stress (σ/σ_r) behavior for each material subjected to FC shows that 70% of the compressive stress was generated between 850 and 710 ºC, i.e., within a variation of ~140 ºC. The numerical simulation showed that this increase of compression stress was expressed straddling the T_g of albite glass, in a narrow temperature range. Furthermore, Figure 14 shows a great influence of the quartz amount on the stress undergone at the surface of the materials. It can be noted at 573 °C that materials containing a large amount of quartz are subjected to high tensile stress on their surface, corresponding to composites D and E.

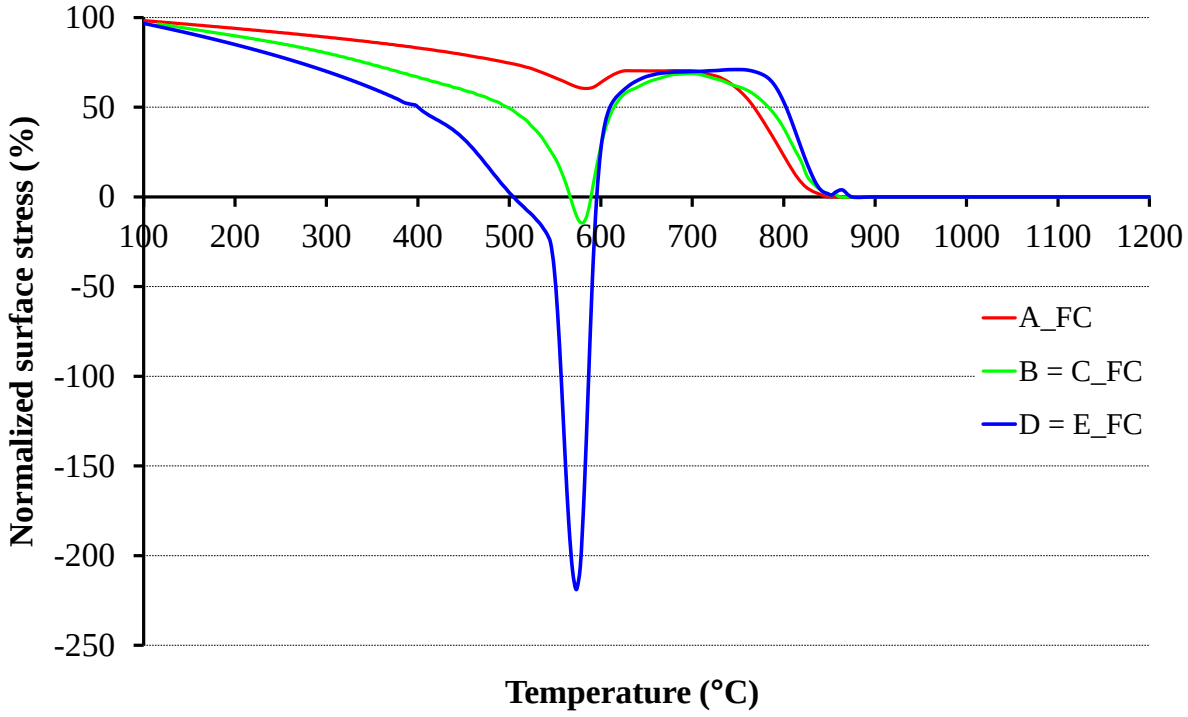

Figure 14. Normalized (σ/σ_r) surface stress variation during fast cooling (FC) for all samples.

During cooling, the specimen supports different kinds of stresses, such as thermal stress and viscoelastic stress. The viscoelastic deformation is accountable for the residual stresses at room temperature because the thermal stress disappears when there is no temperature difference at the specimen cross section. Figure 15 shows the viscoelastic deformation ($\varepsilon_{v,x}$) experienced by material A during FC. Right at the beginning of the FC, the viscoelastic deformation undergoes a large increase, which is observed until the temperature difference between the midplane and surface starts to hold and after it decreases. At this moment, the viscoelastic deformation reaches the maximum, and after that decreases slightly and remains constant up to room temperature. The temperature at which the viscoelastic deformation remains constant is very near the T_g of albite glass, at which the viscosity is ~10^{12} Pa·s [40,41]. This proves that the residual compressive stresses at the surface of the

material originated at temperatures higher than the T_g of the glassy phase, and they are maintained until room temperature due to the increase in viscosity of this phase provided by the gradual decrease in temperature.

From an industrial perspective, although viscoelastic deformation is responsible for the residual stresses of the material after processing, it should be noted that there are several mechanisms that can promote the relaxation of these stresses, such as the occurrence of microstructural defects such as pores and cracks [57]. On the other hand, microstructural stresses are also present, inside and around crystalline particles [58,59]. Despite these parameters not having been incorporated in the numerical methodology of this work, the results of theoretically calculated residual stresses and experimentally measured ones had a good fit. Still, from the industrial point of view, this time related to porcelain tiles, Figure 15 shows that the viscoelastic deformation can be distinguished between the top surface and the bottom surface of the piece. This can be related to problems with delayed curvatures in these materials [60,61].

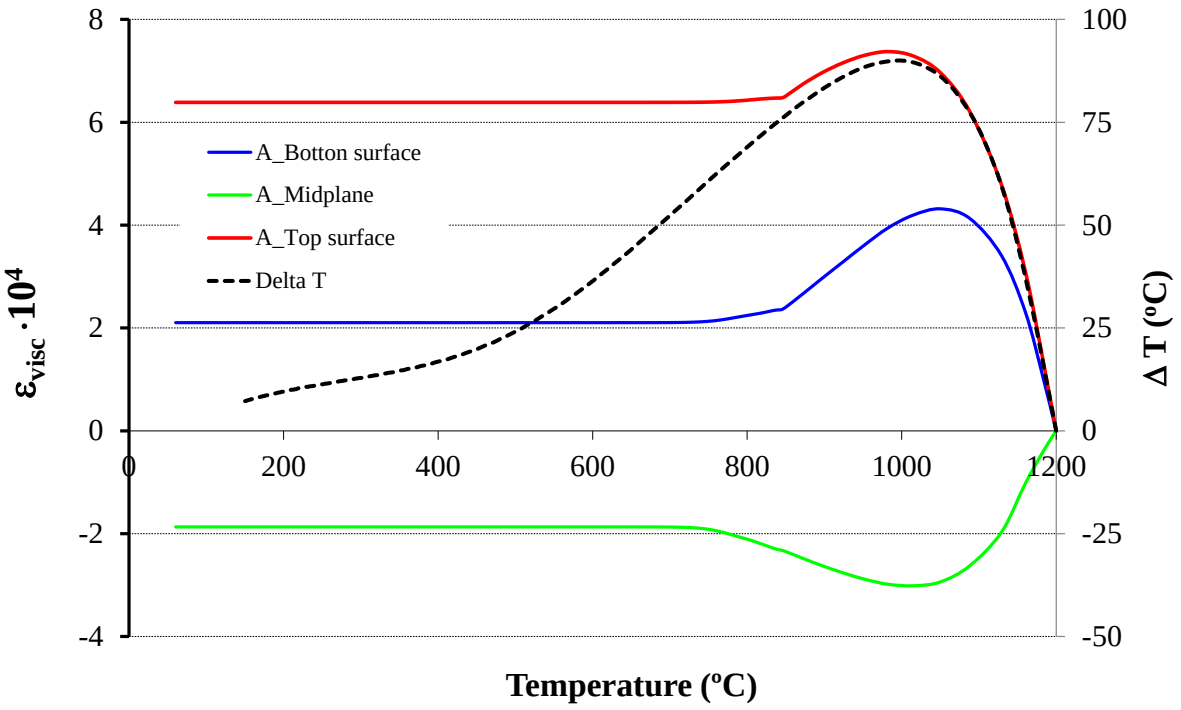

Figure 15. Viscoelastic deformation and temperature difference between midplane and top surface during fast cooling (FC to material A).

Figure 16(a) shows the variation in surface stresses of materials during the quartz β to α transition, subjected to FC. It is noted that an abrupt tensile stress at the surface of the materials occurred close to 573 °C, reaching its maximum value at this temperature. For composites D and E (45.4 wt.% quartz), the numerical simulation results showed that the

surface of the samples was subjected to tensile stresses of ~25 MPa. Within the studied range, the quartz particle size did not influence the stress variation during the quartz transition. On the other hand, the correlation between the fraction of quartz and the variation of tensile stress suffered by the surface of the materials was clear. Figure 16(b) shows the relationship found between the volumetric fraction of quartz and the variation of tensile stress suffered by the surface during the quartz β to α transition. Therefore, according to the numerical simulation, the greater the fraction of quartz in the material, the greater the tensile stress variation undergone by the material's surface during the transition of this crystalline phase.

a) b)

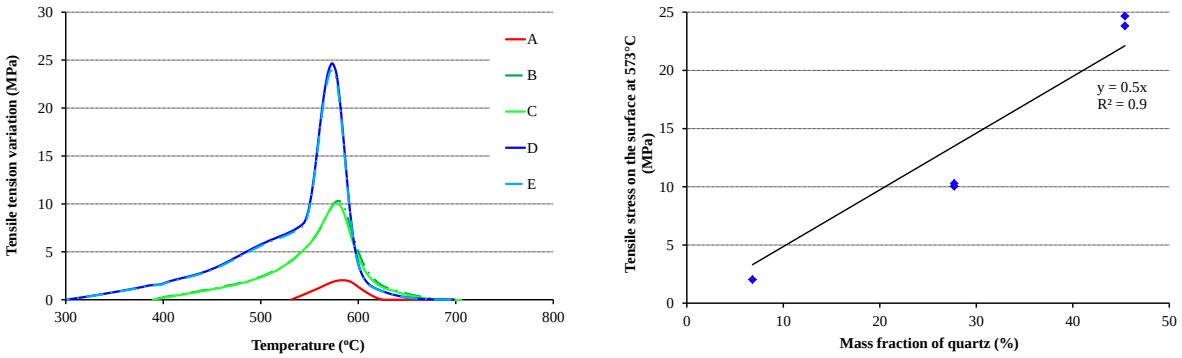

Figure 16. (a) Surface stress variation close to quartz β to α transition and (b) relationship between quartz mass fraction and tensile tension at the surface at 573 °C.

Knowing that the volumetric fraction of quartz helps to generate tensile stress on the surface of the material at temperatures close to the β to α quartz transition (573 °C), it is important to explain what happens macroscopically inside the material. During the quartz transition, when the thermal gradient between the center and the surface is still high (~32 °C for FC), the crystalline quartz particles that are closer to the material surface (top and bottom) undergo an allotropic transition earlier than the particles situated in the center of the material, which still has temperatures above 573 °C. Due to this surface transition, there is a consequent deformation linked to the abrupt volumetric reduction of β to α quartz [59,62,63]. This deformation leads to shrinkage at the material surface, while the center is in a rigid state ($T<T_g \therefore \eta > 10^{12}$ Pa·s), preventing stress relaxation. Consequently, to have a mechanical equilibrium, the surface is subjected to a state of tensile stress (Figure 17). The mathematical model showed that a greater amount of quartz leads to a greater state of tensile stress at the surface of the material during the β to α quartz transition (Figure 13, Figure 14, and Figure 16).

In this sense, the quartz allotropic transition, the amount of crystalline quartz in the composite, and the temperature gradient in the cross section of the material close to 573 °C are the variables that are directly related to the catastrophic fracture due to the thermal shock.

The results of the thermal part of the mathematical model make it possible to obtain the temperature profile in the cross section of the material close to the quartz transition temperature. This simulates the moment when the upper and lower surface of the material is at a temperature lower than 573 °C and the interior still maintains a temperature above 573 °C. Figure 17 shows the thermal gradient at the cross section calculated for the matrix close to the quartz allotropic transition (~573 °C) when subjected to FC. Accordingly, the mechanism for generating internal stresses during this cooling stage is proposed.

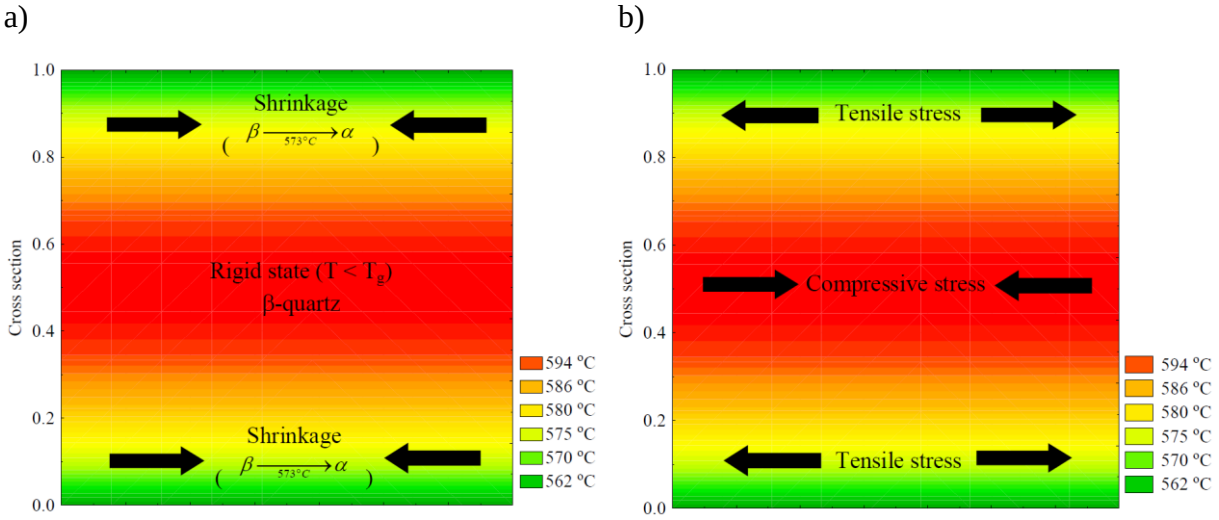

Figure 17. Material A submitted to fast cooling (FC) close to 573 °C: (a) thermal gradient at the cross section; and (b) respective internal stress generation mechanism.

In this case, when the top and bottom surfaces are at 562 °C, the interior of the part is at 594 °C, i.e., the quartz particles near the surface have already undergone the β to α transition, which leads to an abrupt shrinkage of the surface, while the quartz particles located inside the piece still show the β form of crystalline quartz. This abrupt surface shrinkage subjects the material to tensile stress at the surface that, in some cases, can lead to catastrophic fracture.

4.5. Processing-microstructure-properties correlation

Figure 18 shows the microstructure of materials A, B and E submitted to FC. The results show fractures within and around the quartz particles dissolved in the glassy phase. The fracture patterns found in the quartz particles were the same as those found by Gilabert *et*

al. (2012) through numerical simulation of the microstructural stresses involving the quartz particles and the glassy phase [58].

The microstructural characterization showed that fractures within and around the crystalline quartz particles were produced regardless of the percentage and size of the crystalline quartz particles. Previous works showed that microcracks were produced in the microstructure of the materials when there is the presence of crystalline quartz [64]. These microscopic fractures are mainly related to changes in the thermomechanical properties of the quartz crystal linked to its allotropic transition from β to α during the cooling step [65,66].

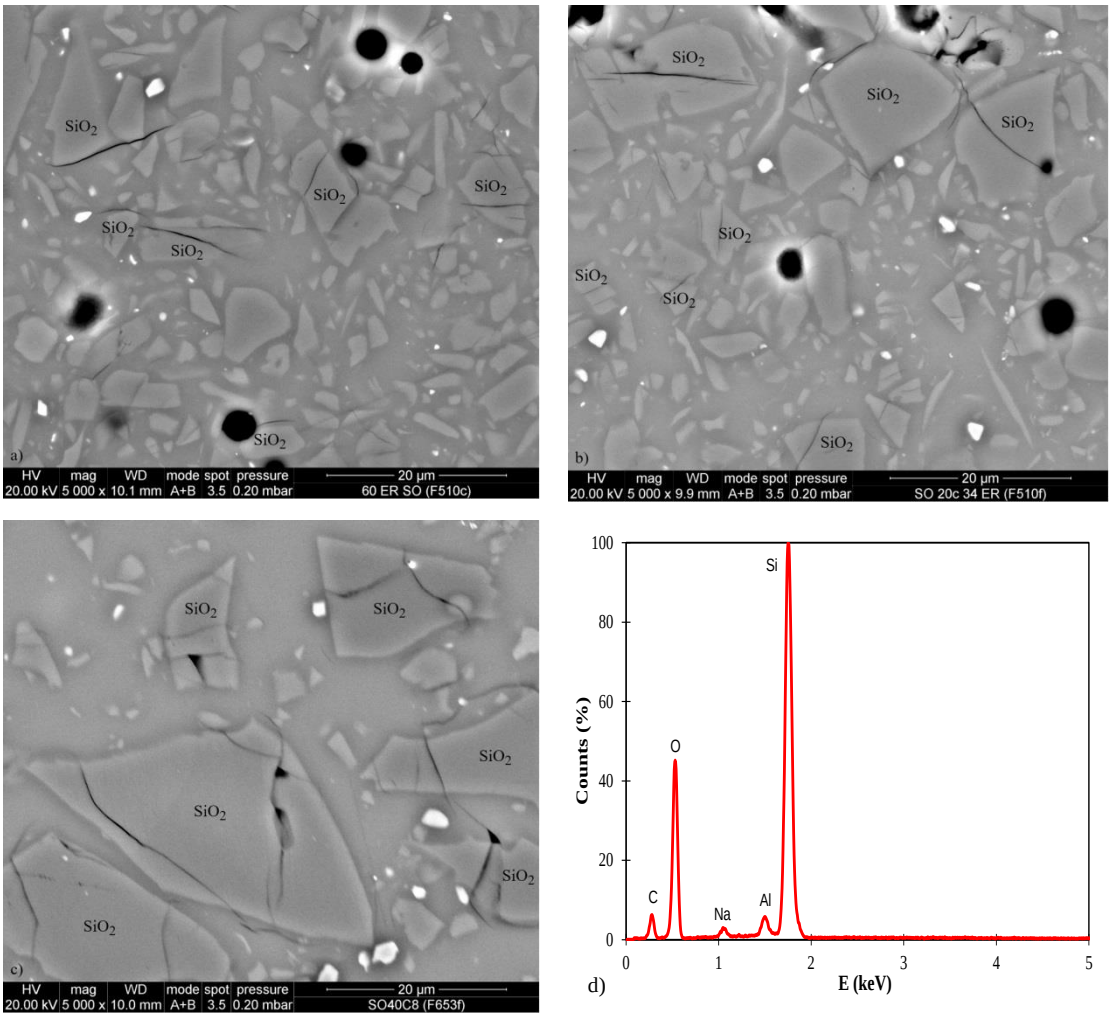

Figure 18. Microstructural evaluation of materials A (a), B (b) and E (c) subjected to FC. Punctual chemical analysis of crystalline quartz particles dissolved in the glassy phase of the materials (d).

5. CONCLUSIONS

In this work, it was possible to predict the evolution and profile of the macroscopic residual stresses in porcelain-like composites based on a feldspar glass matrix with different amounts of quartz particles under different cooling rates. The proposed mathematical model showed good agreement with the experimental results, which were obtained with the Strain Relaxation Slotting Method (SRSM). According to the results, the composites were susceptible to the thermal tempering process, which is generally employed in the manufacturing of glasses, metals, and porcelain materials.

The residual stresses during the different cooling rates (slow, mixed and fast cooling) showed that the high rates increase the residual stresses. A parabolic profile was found for all material compositions and cooling procedures.

Increasing amounts of crystalline quartz particles decreased residual stresses in the surface of the materials. This behavior can be explained by the thermal effective diffusivity increase, respective thermal expansion coefficient decrease at high temperatures, and the viscosity increase according to the Krieger-Dougherty equation. Furthermore, the quartz particle size did not affect the residual stresses. This behavior can be understood because the particle size did not modify the thermomechanical properties at high temperatures. This may be related to the short firing time to which these materials are subjected.

Analyzing the surface stress evolution during the different cooling rates, practically 70% of the stress was increased around a narrow range of temperature between 850 e 710 ºC, i.e., with a variation of ~140 ºC. This range is very near the glass transition temperature (T_g) of the materials studied (816 to 833 ºC).

The quartz β to α transition affected the stress at the cross section of the composite materials. This behavior can be associated with: (*i*) a high temperature gradient between the midplane and surface material during the quartz transition, and (*ii*) variation of the thermomechanical properties of quartz during its allotropic transition. In this case, mainly the decrease in elastic modulus of the quartz particles results in a decrease in the elastic modulus of the ceramic material.

The viscoelastic deformation increased at the beginning of the fast cooling until the temperature difference between the midplane and surface started to decrease. Shortly after that, when the glass viscosity increased, the deformation remained constant until room temperature. The viscoelastic deformation was accountable for the residual stresses at room temperature. This proves that the residual compressive stresses on the surface of the material originate at temperatures higher than the T_g of the glass phase. Those stresses are maintained

until the room temperature is reached due to the increase in viscosity of this phase provided by the gradual decrease in temperature.

The numerical simulation of the behavior of the stress undergone by the surface of the material close to 573 ºC showed the existence of an abrupt tensile stress on the surface of the materials that occurred close to 573 ºC, reaching its maximum value at this temperature. For materials with 45.4 wt.% quartz, the samples were subjected to tensile stresses reaching ~25 MPa. Within the studied range, the quartz particle size did not influence the stress variation during the quartz transition. A linear relationship between the quartz volumetric fraction and the tensile stress occurred at the surface of the material at 573 ºC.

In that regard, the β to α transition of quartz, the amount of quartz in the sample, and the temperature gradient in the cross section of the material close to 573 ºC are the variables that are closely related to the catastrophic fracture of the material due to thermal shock.

Finally, tensile stresses on the surface of the material and the generation of microcracks within and around the quartz particles at ~573 ºC may contribute to catastrophic fracture of the material due to thermal shock during the cooling step.

Acknowledgments

This work was financially supported by the Ministry of Science and Innovation, within the National Program for Fundamental Research Projects (BIA2009-10692), and by the project CAPES-DGU (BEX 6505/10-4).

References

[1] W.M. Carty, U. Senapati, Porcelain - raw materials, processing, phase evolution, and mechanical behavior, J. Am. Ceram. Soc. 81(1) (1998) 3-20. https://doi.org/10.1111/j.1151-2916.1998.tb02290.x.

[2] R.W. Davidge, Thermal Shock, in: R.J. Brook (Ed.), Concise Encyclopedia of Advanced Ceramic Materials, Pergamon, Oxford, 1991, pp. 478-481. https://doi.org/10.1016/B978-0-08-034720-2.50132-5.

[3] O.S. Narayanaswamy, R. Gardon, Calculation of residual stresses in glass, J. Am. Ceram. Soc. 52(10) (1969) 554-558. https://doi.org/10.1111/j.1151-2916.1969.tb09163.x.

[4] R. Gardon, Thermal Tempering of Glass, Elasticity and Strength in Glasses: Glass: Science and Technology, Elsevier Science, 2012.

[5] D.J. Green, Y. Khalfalla, K.Y. Benyounis, A.N.M. Karim, Ceramics and Glasses, Tempering of Residual Stresses, Reference Module in Materials Science and Materials Engineering, Elsevier, 2019. https://doi.org/10.1016/B978-0-12-803581-8.03377-4.

[6] A. Talimian, V.M. Sglavo, Glass: Chemical and Thermal Strengthening, in: M. Pomeroy (Ed.), Encyclopedia of Materials: Technical Ceramics and Glasses, Elsevier, Oxford, 2021, pp. 632-646. https://doi.org/10.1016/B978-0-12-818542-1.00075-8.

[7] A. De Noni Jr., D. Hotza, V. Cantavella, E. Sanchez, Influence of macroscopic residual stresses on the mechanical behavior and microstructure of porcelain tile, J. Eur. Ceram. Soc. 28(13) (2008) 2463-2469. https://doi.org/10.1016/j.jeurceramsoc.2008.03.003.

[8] A. De Noni Jr., D. Hotza, V. Cantavella, E.S. Vilches, Influence of Composition on Mechanical Behaviour of Porcelain Tile. Part I: Microstructural Characterization and Developed Phases After Firing, Materials Science and Engineering: A 527(7–8) (2010) 1730-1735. https://doi.org/10.1016/j.msea.2009.10.057.

[9] A. De Noni Jr., D. Hotza, V. Cantavella, E.S. Vilches, Influence of Composition on Mechanical Behaviour of Porcelain Tile. Part II: Mechanical Properties and Microscopic Residual Stress, Materials Science and Engineering: A 527(7–8) (2010) 1736-1743. https://doi.org/10.1016/j.msea.2009.10.060.

[10] A. De Noni Jr., D. Hotza, V.C. Soler, E.S. Vilches, Influence of composition on mechanical behaviour of porcelain tile. Part III: Effect of the cooling rate of the firing cycle, Mater. Sci. Eng. A 528(9) (2011) 3330-3336. https://doi.org/10.1016/j.msea.2010.12.086.

[11] K. Asaoka, N. Kuwayama, J.A. Tesk, Influence of tempering method on residual stress in dental porcelain, Journal of dental research 71(9) (1992) 1623-1627. https://doi.org/10.1177/00220345920710091501.

[12] P.H. DeHoff, K.J. Anusavice, Analysis of tempering stresses in bilayered porcelain discs, Journal of dental research 71(5) (1992) 1139-44. https://doi.org/10.1177/00220345920710050201.

[13] T. Chartier, D. Merle, J.L. Besson, Laminar ceramic composites, J. Eur. Ceram. Soc. 15(2) (1995) 101-107. https://doi.org/10.1016/0955-2219(95)93055-8.

[14] L.L. Shaw, Thermal residual stresses in plates and coatings composed of multi-layered and functionally graded materials, Compos Part B-Eng 29(3) (1998) 199-210. https://doi.org/10.1016/S1359-8368(97)00029-2.

[15] H. Hahn, K.-S. Kim, R. Croman, The effect of cooling rate on residual stress in a thermoplastic composite, J. Compos. Tech. Res. 11(2) (1989) 47-52.

[16] T.J. Chapman, J.W. Gillespie, R.B. Pipes, J.-A.E. Månson, J.C. Seferis, Prediction of process-induced residual stresses in thermoplastic composites, J. Compos. Mater. 24(6) (1990) 616-643. https://doi.org/10.1177/002199839002400603.

[17] K.R.V. Horn, Residual stresses introduced during metal fabrication, J. Met. 197 (1953) 405-422

[18] D.Y. Jang, T.R. Watkins, K.J. Kozaczek, C.R. Hubbard, O.B. Cavin, Surface residual stresses in machined austenitic stainless steel, Wear 194(1) (1996) 168-173. https://doi.org/10.1016/0043-1648(95)06838-4.

[19] V. Cantavella, A. Moreno, A. Mezquita, J.C. Jarque, J. Barberá, A. Palanques, Evolution of stresses and curvatures in porous bodies during cooling, X Congreso mundial de la calidad del azulejo y del pavimento cerámico - Qualicer 2008, Cámara oficial de comercio, industria y navegación, Castellón de La Plana, Spain, 2008, pp. P.BC241-P.BC255.

[20] F.P. Incropera, D.P.d. Witt, Fundamentals of Heat and Mass Transfer, John Wiley & Sons, Singapore, 1990.

[21] A.S. Quiroga, Course of Elasticity, Bellisco, Madrid, 1990.

[22] J. Lu, Handbook of Measurement of Residual Stresses, Prentice Hall, 1996.

[23] M.B. Prime, Residual stress measurement by successive extension of a slot: The crack compliance method, Appl. Mech. Rev. 52(2) (1999) 75-96. https://doi.org/10.1115/1.3098926.

[24] C.C. Aydiner, E. Üstündag, M.B. Prime, A. Peker, Modeling and measurement of residual stresses in a bulk metallic glass plate, J. Non. Cryst. Solids 316(1) (2003) 82-95. https://doi.org/10.1016/s0022-3093(02)01940-3.

[25] A. De Noni Jr., Estudo das propriedades mecânicas de porcelanato através da avaliação de tensões residuais microscópicas e macroscópicas originadas durante a etapa de resfriamento do ciclo de queima, Departamento de Pós-Graduação em Ciência e Engenharia de Materiais, UFSC, Florianópolis/SC, 2007.

[26] C.M. Scarfe, D.J. Cronin, Viscosity-temperature relationships of metls at 1atm in the system diopside-albite, Am. Mineral. 71(5-6) (1986) 767-771.

[27] W.D. Kingery, Factors affecting thermal stress resistance of ceramic materials, J. Am. Ceram. Soc. 38(1) (1955) 3-15. https://doi.org/10.1111/j.1151-2916.1955.tb14545.x.

[28] H.T. Davis, L.R. Valencourt, C.E. Johnson, Transport processes in composite media, J. Am. Ceram. Soc. 58(9-10) (1975) 446-452. https://doi.org/10.1111/j.1151-2916.1975.tb19020.x.

[29] R. Landauer, The Electrical Resistance of Binary Metallic Mixtures, AIP, 1952.

[30] J.K. Carson, S.J. Lovatt, D.J. Tanner, A.C. Cleland, Thermal conductivity bounds for isotropic, porous materials, Int. J. Heat Mass. Tran. 48(11) (2005) 2150-2158. https://doi.org/10.1016/j.ijheatmasstransfer.2004.12.032.

[31] A. Hofmeister, A. Whittington, M. Pertermann, Transport properties of high albite crystals, near-endmember feldspar and pyroxene glasses, and their melts to high temperature, Contrib. Mineral Petr. 158(3) (2009) 381-400. https://doi.org/10.1007/s00410-009-0388-3.

[32] B. Gibert, D. Mainprice, Effect of crystal preferred orientations on the thermal diffusivity of quartz polycrystalline aggregates at high temperature, Tectonophysics 465(1-4) (2009) 150-163. https://doi.org/10.1016/j.tecto.2008.11.006.

[33] R.C. Weast, Handbook of Chemistry and Physics, CRC Press, Cleveland, OH, 1974.

[34] I. Ohno, K. Harada, C. Yoshitomi, Temperature variation of elastic constants of quartz across the α - β transition, Phys. Chem. Miner. 33(1) (2006) 1-9. https://doi.org/doi.org/10.1007/s00269-005-0008-3.

[35] B.S. Hemingway, Quartz; heat capacities from 340 to 1000 K and revised values for the thermodynamic properties, Am. Mineral. 72(3-4) (1987) 273-279.

[36] T. Rouxel, Elastic properties and short-to medium-range order in glasses, J. Am. Ceram. Soc. 90(10) (2007) 3019-3039. https://doi.org/10.1111/j.1551-2916.2007.01945.x.

[37] G.I. Taylor, The viscosity of a fluid containing small drops of another fluid, Proceedings of the Royal Society of London. Series A, containing papers of a mathematical and physical character 138(834) (1932) 41-48.

[38] I.M. Krieger, T.J. Dougherty, A mechanism for non-newtonian flow in suspensions of rigid spheres, SOR, 1959.

[39] M. Wang, N. Pan, Predictions of effective physical properties of complex multiphase materials, Mat. Sci. Eng. R. 63(1) (2008) 1-30. https://doi.org/10.1016/j.mser.2008.07.001.

[40] F. Magrini, R. Ferrari, P. Brunetti, The role of viscosity and surface tension in the firing of glazes and ceramic glazes, Ceram. Inf. 171 (1979).

[41] E. Neves, E.D. Poffo, M.C. Fredel, H.G. Riella, O.E. Alarcon, Effect of addition of Na_2O in viscosity and devitrification of the glass obtained from fly ash Li_2O, Quím. Nova 21(4) (1998) 534-537.

[42] V. Cantavella, A. Moreno, A. Mezquita, D. Llorens, J. Barberá, A. Palanques, Distribución de temperaturas en el interior de una pieza durante la cocción industrial, IX

Congreso mundial de la calidad del azulejo y del pavimento cerámico, Qualicer 2006, AICE, Castellón - Spain, 2006, pp. P.BC 151-164.

[43] ASTM, E1876-09 Physical Testing Standards and Mechanical Testing Standards, Standard test method for dynamic Young's modulus, shear modulus, and Poisson's ratio by impulse excitation of vibration, ASTM International, 2009. https://doi.org/10.1520/E1876-21.

[44] C.S. Montross, Elastic modulus versus bond length in lanthanum chromite ceramics, J. Eur. Ceram. Soc. 18(4) (1998) 353-358. https://doi.org/10.1016/s0955-2219(97)00143-x.

[45] W. Lemmens, Dynamic measurements in materials, American Society for Testing and Materials, Philadelphia, 1990.

[46] D. Lakshtanov, S. Sinogeikin, J. Bass, High-temperature phase transitions and elasticity of silica polymorphs, Phys Chem Miner 34(1) (2007) 11-22. https://doi.org/10.1007/s00269-006-0113-y.

[47] I. Ahrens, Mineral Physics and Crystallography: A Handbook of Physical Constants, American Geophysical Union, Washington, 1995.

[48] M. Dal Bó, V. Cantavella, E. Sánchez, D. Hotza, F.A. Gilabert, Fracture toughness and temperature dependence of Young's modulus of a sintered albite glass, J. Non-Cryst. Solids 363(0) (2013) 70-76. http://dx.doi.org/10.1016/j.jnoncrysol.2012.12.001.

[49] A.P.N. Oliveira, E.S. Vilches, V.C. Soler, F.A.G. Villegas, Relationship between Young's modulus and temperature in porcelain tiles, J. Eur. Ceram. Soc. 32(11) (2012) 2853-2858. https://doi.org/10.1016/j.jeurceramsoc.2011.09.019.

[50] P.H. DeHoff, K.J. Anusavice, Tempering stresses in feldspathic porcelain, Journal of dental research 68(2) (1989) 134-8. https://doi.org/10.1177/00220345890680020701.

[51] E. Sánchez, V. Sanz, J. Castellano, J. Sales, K. Kayacı, M.U. Taşkıran, Ü.E. Anıl, Ş. Türk, Residual stresses in porcelain tiles. Measurement and process variables assessment, J. Eur. Ceram. Soc. (2019). https://doi.org/10.1016/j.jeurceramsoc.2019.04.038.

[52] J.H. Nielsen, K. Thiele, J. Schneider, M.J. Meyland, Compressive zone depth of thermally tempered glass, Construction and Building Materials 310 (2021) 125238. https://doi.org/10.1016/j.conbuildmat.2021.125238.

[53] J.H. Nielsen, Remaining stress-state and strain-energy in tempered glass fragments, Glass Structures & Engineering 2(1) (2017) 45-56. https://doi.org/10.1007/s40940-016-0036-z.

[54] N. Pourmoghaddam, M.A. Kraus, J. Schneider, G. Siebert, Relationship between strain energy and fracture pattern morphology of thermally tempered glass for the prediction of the 2D macro-scale fragmentation of glass, Glass Structures & Engineering 4(2) (2019) 257-275. https://doi.org/10.1007/s40940-018-00091-1.

[55] A. De Noni Jr., D. Hotza, V. Cantavella, E.S. Vilches, Influencia del enfriamiento de la etapa de cocción sobre las propiedades mecánicas del gres porcelánico, Bol. Soc. Esp. Ceram. V. 46(4) (2007) 163-170. https://doi.org/10.3989/cyv.2007.v46.i4.231.

[56] V. Cantavella, E. Sánchez, A.D.N. Junior, D. Hotza, Influence of macrostresses and microstresses on the mechanical behaviour of porcelain tiles, in: E.G. Verlag (Ed.) Proceedings of the 10th international conference of the European Ceramic Society (ECerS), Berlin, Germany, 2008.

[57] A.G. Lanin, Effect of residual stresses on the strength of ceramic materials (Review), Russian Metallurgy (Metally) 2012(4) (2012) 307-322. http://dx.doi.org/10.1134/S0036029512040076.

[58] F.A. Gilabert, M. Dal Bó, V. Cantavella, E. Sánchez, Fracture patterns of quartz particles in glass feldspar matrix, Mater Lett 72(0) (2012) 148-152. http://dx.doi.org/10.1016/j.matlet.2011.12.074.

[59] F.A. Gilabert, V. Cantavella, M. Dal Bó, E. Sánchez, Modeling microstructural damage of silicate-based ceramics and its influence on macroscopic fracture strength, Acta Mater. 70 (2014) 30-44. https://doi.org/10.1016/j.actamat.2014.01.026.

[60] V. Cantavella, J. García-Ten, E. Sánchez, E. Bannier, J. Sánchez, C. Soler, J. Sales, Delayed curvatures in porcelain tile. Analysis and measurement of influencing factors, X Congreso mundial de la calidad del azulejo y del pavimento cerámico - Qualicer 2008, Castellón, 2008, pp. P.BC207-P.BC224.

[61] E. Bannier, J. García-Ten, J. Castellano, V. Cantavella, Delayed curvature and residual stresses in porcelain tiles, J Eur Ceram Soc 33(3) (2013) 493-501. http://dx.doi.org/10.1016/j.jeurceramsoc.2012.09.018.

[62] A.H. Jay, The Thermal Expansion of Quartz by X-Ray Measurements, Proceedings of the Royal Society of London. Series A 142(846) (1933) 237-247. https://doi.org/10.1098/rspa.1933.0165.

[63] S. Tsuneyuki, H. Aoki, M. Tsukada, Y. Matsui, Molecular-dynamics study of the α to β structural phase transition of quartz, Phys. Rev. Lett. 64(7) (1990) 776-779. https://doi.org/10.1103/PhysRevLett.64.776.

[64] M. Knapek, T. Húlan, P. Minárik, P. Dobroň, I. Štubňa, J. Stráská, F. Chmelík, Study of microcracking in illite-based ceramics during firing, Journal of the European Ceramic Society 36(1) (2016) 221-226. https://doi.org/10.1016/j.jeurceramsoc.2015.09.004.

[65] Y.M. Ito, M. Rosenblatt, L.Y. Cheng, F.F. Lange, A.G. Evans, Cracking in particulate composites due to thermalmechanical stress, International Journal of Fracture 17(5) (1981) 483-491. http://dx.doi.org/10.1007/bf00033343.

[66] F. Chmelík, A. Trník, I. Štubňa, J. Pešička, Creation of microcracks in porcelain during firing, Journal of the European Ceramic Society 31(13) (2011) 2205-2209. http://dx.doi.org/10.1016/j.jeurceramsoc.2011.05.045.